JACS
JOURNAL OF THE AMERICAN CHEMICAL SOCIETY
Article
pubs.acs.org/JACS

How Surface Potential Determines the Kinetics of the First Hole Transfer of Photocatalytic Water Oxidation

Matthias M. Waegele,[†] Xihan Chen,[†] David M. Herlihy,[†] and Tanja Cuk*[,†,‡]

[†]Department of Chemistry, University of California, Berkeley, Berkeley, California 94720, United States
[‡]Chemical Sciences Division, Lawrence Berkeley National Laboratory, Berkeley, California 94720, United States

Supporting Information

ABSTRACT: Interfacial hole transfer between n-$SrTiO_3$ and OH^- was investigated by surface sensitive transient optical spectroscopy of an in situ photoelectrochemical cell during water oxidation. The kinetics reveal a single rate constant with an exponential dependence on the surface hole potential, spanning time scales from 3 ns to 8 ps over a ≈1 V increase. A voltage- and laser illumination-induced process moves the valence band edge at the n-type semiconductor/water interface to continuously change the surface hole potential. This single step of the water oxidation reaction is assigned to the first hole transfer $h^+ + OH^- \rightarrow OH^\bullet$. The kinetics quantify how much a change in the free energy difference driving this first hole transfer reduces the activation barrier. They are also used to extrapolate the kinetic rate due to the activation barrier when that free energy difference is zero, or the Nernstian potential. This is the first time transient spectroscopy has enabled the separation of the first hole transfer from the full four hole transfer cycle and a direct determination of these two quantities. The Nernstian potential for $OH^-/OH^\bullet$ is also suggested, in rough agreement with gas-phase studies. The observation of a distinct, much longer time scale upon picosecond hole transfer to OH^- suggests that a dominant, more stable intermediate of the water oxidation reaction, possibly a surface bound oxo, may result.

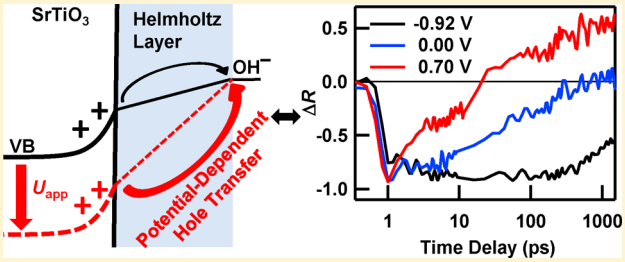

INTRODUCTION

Water oxidation at solid metal oxide photocatalysts of earth abundant metals is a highly selective heterogeneous chemical reaction for O_2 evolution whose mechanism is of intense current interest.[1−16] The motivation to understand this catalytic process step-by-step is based on the fact that it is an indispensable part of any renewable fuel forming reaction, and solid oxides are particularly active catalyst materials. Insights gained from uncovering elementary charge-transfer processes and how they couple to chemical transformation at the catalyst/water interface are key for the design of more efficient catalysts. As suggested by calibrated photochemical studies, the full cycle involves four hole transfers from the catalyst to water.[4,17,18] Under basic conditions, hydroxyl groups are more easily oxidized, such that

$$4h^+ + 4OH^- \rightarrow O_2 + 2H_2O \quad (1)$$

The challenge is to follow the kinetics of each hole transfer and the formation and lifetime of the intermediate species of the catalytic cycle that result. In turn, this will identify the hole transfer(s) that limit the reaction rate and the more facile hole transfer(s) that dynamically alter the catalytic surface for the rate limiting step(s). In photochemical or electrochemical studies, the dependence of steady-state product evolution on the free energy difference driving the hole transfer is used to extract activation barriers.[6,15] While providing insight into the mechanism, these steady-state studies are highly model dependent for multistep reactions.[19,20] Only the transient response of the photodriven water oxidation reaction can directly step through a catalytic cycle. In particular, ultrafast spectroscopy, by following the reaction from time zero can most readily differentiate the kinetics of the disparate physical processes involved. The initial step in the cycle is the first hole transfer and is suggested to involve the following reaction in basic conditions:

$$h^+ + OH^- \rightarrow OH^\bullet \quad (2)$$

where $OH^\bullet$ is a hydroxyl radical that may either be bound to a metal ion at the surface or be free in solution. A more stable metal oxo intermediate is likely to be formed from this unstable radical, as suggested by steady-state electrochemical studies[3,6,15,21,22] and the recent millisecond time scale infrared studies that saw the oxo intermediate directly.[8,16]

Ultrafast transient optical spectroscopy of the photodriven water oxidation reaction at the n-type semiconductor/water interface in principle could follow the kinetics of this first hole transfer. Here, the photogenerated holes are efficiently separated within the semiconductor and sent to the aqueous interface at femtosecond time scales, defining the starting point of the cycle. However, so far, the kinetics that apply to the first hole transfer have not been differentiated from subsequent

Received: April 10, 2014
Published: July 16, 2014

   dx.doi.org/10.1021/ja503603k | J. Am. Chem. Soc. 2014, 136, 10632−10639

kinetic steps. Transient optical spectroscopy has assigned a range of interfacial hole transfer time constants from 500 ps[1,2] to hundreds of ms[4,7] at the n-TiO_2 and n-Fe_3O_4 aqueous interfaces. Many of these studies were conducted under conditions where the quantum efficiency of O_2 evolution is low (0.1% to 5%),[4,10] such that the true interfacial kinetics is difficult to separate from electron−hole recombination kinetics within the semiconductor. Further, these studies were conducted at a single surface hole potential, determined by the valence band edge at the aqueous interface.[23−27] Therefore, the kinetics could not be followed as a function of the free energy difference between the reactants and products. This prevents attributing the kinetics to a single step of the reaction and understanding its activation barrier through a tunable free energy.

Herein we report on transient optical spectroscopy of n-$SrTiO_3$ in an in situ electrochemical cell under conditions of high quantum efficiency (>75%) and surface sensitivity (≈25 nm) that reveals the kinetics of interfacial hole transfer as a function of the surface hole potential. n-$SrTiO_3$ is a representative transition metal oxide-based photoanode and is ideally suited for time-resolved pump−probe spectroscopy due to its high-quantum efficiency for O_2 evolution with 300 nm excitation. Continuous tuning of the surface hole potential on the electrochemical cell is achieved by a voltage- and laser-induced process[26,28] that moves the position of the valence band edge at the aqueous interface with the applied potential on the electrochemical cell.

The kinetics reveal a single rate constant with an exponential dependence on the surface hole potential, spanning time scales from 3 ns to 8 ps over a ≈1 V increase. This indicates that we are mapping an activation barrier for a single step of the water oxidation reaction, differentiating the first hole transfer from the rest. The activation barrier for this first hole transfer, suggested to be the $OH^-/OH^•$ reaction, is quantified by a hole transfer coefficient, α, that determines how efficiently increasing the free energy difference reduces the activation barrier and by a rate constant, k_0, that relates to its magnitude when the free energy difference is zero, or the Nernstian potential. Further, the data also suggest a Nernstian potential for the $OH^-/OH^•$ reaction in solution that is in rough agreement with gas-phase studies in a hydrated environment, supporting the assignment of reaction 2 to the initial step of the water oxidation reaction and to the kinetics being probed here. Following the first hole transfer, the kinetics reveal a much longer time scale, possibly related to the formation of a metal oxo intermediate and further showing that multiple steps of the cycle can be differentiated.

EXPERIMENTAL PROCEDURES

The 0.7% and 0.08% Nb-doped $SrTiO_3$ by weight (henceforth referred to as 0.7% and 0.1%, respectively) single crystals with crystallographic orientation (100) were obtained from MTI Corp. (Richmond, CA). The crystals were 0.5 mm thick with polished front sides (R_a < 5 Å) and unpolished back sides. All spectroscopic measurements were performed on the polished front sides.

The optical constants of Nb-doped $SrTiO_3$ were derived from spectroscopic ellipsometry measurements recorded on a Horiba Jobin-Yvon UVISEL Ellipsometer (Horiba, Edison, NJ). The spectra were taken in reflection mode in air at a 70° angle of incidence.

All spectroelectrochemical measurements were performed in a Teflon electrochemical cell with CaF_2 optical windows (3 mm thick). The electrolyte was a ≈0.1 M aqueous solution of sodium hydroxide for all experiments, unless otherwise noted. To avoid formation of laser-induced air bubbles during pump−probe experiments, electrolyte solutions were briefly degassed under vacuum before commencing experimental measurements. The amount of laser light was insufficient to generate a macroscopically observable O_2 bubble. Bubble formation was solely due to above-band gap excitation of $SrTiO_3$, which heated the solution in the vicinity of the semiconductor/electrolyte interface, thereby liberating dissolved gases. The electrolyte was in contact with the atmosphere during measurements. The potential of the n-$SrTiO_3$ working electrode with respect to an Ag/AgCl reference electrode (MF-2052; Basi, West Lafayette, IN) was controlled by a CHI1140B Potentiostat (CH Instruments, Austin, TX). A Pt wire served as the counter electrode. Ohmic contact between the unpolished n-$SrTiO_3$ back side and copper wire was established using silver paste (Electron Microscopy Sciences, Hatfield, PA). For the transient reflectance experiments, an insulating lacquer covered all surfaces except the polished front side of the crystal. The exposed front surface areas of the 0.1% and 0.7% Nb-doped samples were ≈25 and ≈50 mm^2, respectively. For differential capacitance measurements, the exposed front side area was matched to the Gaussian laser spot size of ≈1 mm^2 (fwhm).

Differential capacitance measurements were carried out using ac voltammetry. The dc potential was swept from positive to negative applied potentials. The ac amplitude and frequency were 0.025 V and 100 Hz, respectively.

For the transient reflectance experiments, the pump and probe beams were derived from a regeneratively amplified Ti:sapphire laser system (Coherent Legend; Coherent, Inc., Santa Clara, CA) producing output pulses with a center wavelength of 800 nm and ≈150 fs temporal width at a 1 kHz repetition rate. Part of the amplifier output was directed into an optical parametric amplifier (OPerA-SOLO; Light Conversion, Vilnius, Lithuania) for generation of laser pump pulses at 300 nm. The s-polarized 800 nm probe beam was directed onto the sample at a 45° incident angle. The pump beam, perpendicularly polarized to the probe beam, was incident normal to the sample surface. After the sample, the reflected probe beam was focused into an optical fiber, which was coupled to a CCD array spectrometer (CAM-VIS-3; Ultrafast Systems, LLC, Sarasota, FL). In all experiments, the pump beam was modulated by a mechanical chopper (3501; Newport, Inc., Irvine, CA) at a frequency of 500 Hz. The detector output was interfaced with a personal computer, which provided automated control over an optical pump−probe delay stage (MTM250CC1; Newport, Inc., Irvine, CA). Typical pump-induced reflectance changes ($\Delta R/R$) were on the order of 0.8 mOD. The typical incident pump fluence was about 0.045 mJ cm^{-2}, corresponding to carrier densities on the order of 10^{19} cm^{-3}. The excitation beam spot size was ≈500 μm (fwhm).

Under conditions of 150 fs pulsed laser excitation and current flow, the sample damages. The damage was investigated by scanning electron microscopy (Figure S1, Supporting Information). While otherwise displaying the flat surface of the single crystal sample, the images show pits in the sample on the order of 5−10 μm in diameter covering about 15% of the surface. These randomly located pits indicate ablation of the material. The most commonly reported cause of such laser-induced material ablation is Coulomb explosion.[29,30] In this process, enough charge is deposited in the material such that bonds are broken. In our experimental conditions, each laser pulse produces ≈10^{19} holes/cm^3 in the depletion layer that could cause bond breaking if the same area is traversed by subsequent pulses and the water oxidation reaction has not yet depleted the stored charge. To minimize this damage, the transient experiments were performed on a moving sample at each time point at open circuit conditions, where no damage took place, and closed circuit conditions of current flow, where damage did take place.

The overall voltammogram did not appreciably change during the course of the experiment, indicating that the catalyst was chemically stable and further signifying that the damage was caused by a physical process in which microscopic pieces of materials are explosively removed, and not due to a progressive chemical reaction consuming the electrode material. Indeed, previous experiments on n-$SrTiO_3$ with high current densities performed over many hours do not exhibit chemical photocorrosion in basic conditions.[31,32]

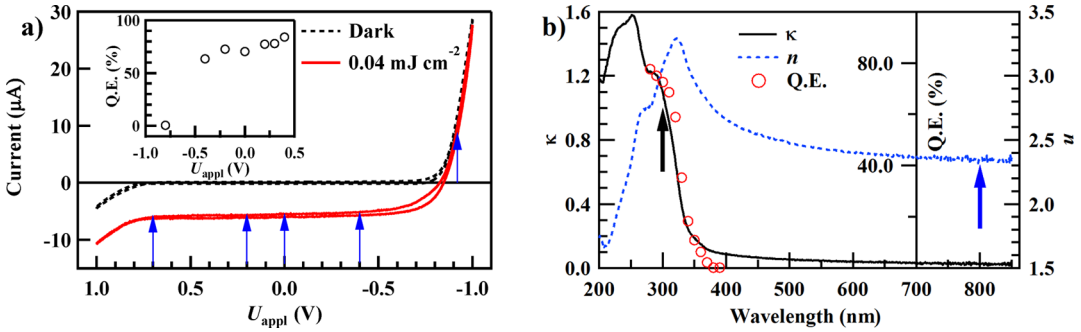

Figure 1. (a) Current−voltage curves of n-$SrTiO_3$ with and without laser irradiation. The blue arrows indicate the voltages at which transient kinetics were measured. The inset shows the quantum efficiency under laser irradiation. (b) Imaginary (κ) and real (n) parts of the complex index of refraction of n-$SrTiO_3$. The open circles show the quantum efficiency (Q.E.) of the photocurrent at U_{appl} = 0 V. The output of a monochromatized xenon lamp was used as an excitation source. The arrows indicate the excitation wavelength (300 nm) and probe wavelength (800 nm) employed in the time-resolved experiments.

RESULTS

Steady-State Current: O_2 Evolution. n-$SrTiO_3$ is a model system for studying the kinetics of O_2 evolution by transient optical spectroscopy. It exhibits a near ideal photoinduced current for an n-type semiconductor and a very high quantum efficiency for the reaction. Since the kinetic measurements herein focus on 0.1% Nb-doped $SrTiO_3$, we primarily report on that sample and use 0.7% Nb-doped $SrTiO_3$ to verify the trends in the data.

Figure 1a shows the results of steady-state current measurements with n-$SrTiO_3$ as the photoanode in an electrochemical cell in the dark and with 500 Hz, 150 fs laser excitation at 300 nm. The current versus voltage curve exhibits an ideal diode-like behavior. For cathodic voltages more negative than −0.8 V the n-type semiconductor is in a forward bias regime where the surface electric field that separates the electron−hole pairs (depletion layer) decreases in width and the current exponentially decays to zero. Under anodic voltages, the semiconductor is largely in a reverse-bias regime where the width of the depletion layer is maximized and the anodic current is largely potential-independent.

Both the shape of this curve and the quantum efficiency of the photocurrent (>75%), defined as the ratio of the photocurrent to the absorbed light flux, are similar to that obtained with a continuous xenon lamp source (Figure 1b and Figure S2, Supporting Information). The photocurrent measurements are conducted in a regime of high pH (11−14), where the steady-state current is independent of pH and not considered mass diffusion limited (Figure S3, Supporting Information).[19]

The high quantum efficiency is achieved by ensuring that the excitation absorption depth, $d = \lambda/4\pi\kappa$, where λ is the excitation wavelength and κ is the imaginary part of the refractive index, is smaller than or equal to the width of the depletion layer. As shown in Figure 1b, where the quantum efficiency is plotted together with the index of refraction as a function of wavelength, the quantum efficiency closely follows κ. Using the Schottky approximation for the n-type semiconductor/liquid interface, the depletion width is given according to[27]

$$W = \sqrt{\frac{2\epsilon\epsilon_0}{|e_0|N_d}\left(U_{SC} - \frac{k_B T}{|e_0|}\right)} \quad (3)$$

where N_d, ϵ_0, ϵ, e_0, k_B, and T represent the doping density, the vacuum permittivity, the dielectric constant of the semiconductor, the electronic charge, the Boltzmann constant, and the absolute temperature, respectively. Using a value of 0.85 V for the voltage drop in the semiconductor (U_{SC}) determined by photovoltage measurements described below, the depletion width is calculated to be ≈25 nm and matches the absorption depth, d, of 300 nm light.

Helmholtz Voltage: Valence Band Edge Motion. At the solid/liquid interface of an n-type semiconductor, any voltage drop across the interface is distributed across both the semiconductor depletion layer (U_{SC}) and the Helmholtz layer (U_H) as shown in Figure 2.[23−27] The Helmholtz layer comes

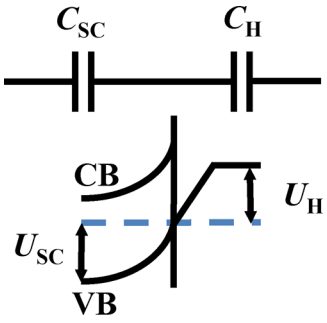

Figure 2. Diagram of the distribution of voltage between the Helmholtz capacitance (C_H) and semiconductor (depletion layer) capacitance (C_{SC}).

from negative ions in the liquid screening the positive charge in the semiconductor,[23−25] forming a very thin parallel plate capacitor at the interface. U_H is therefore defined to be the voltage drop between the valence band edge potential at the interface and the solution potential. In an electrochemical cell, the voltage drop comes from both the applied voltage (U_{appl}) and the flatband voltage determined by equilibration of the chemical potentials of the semiconductor and the liquid (U_{fb}), leading to the following equation:[24,25]

$$U_{appl} - U_{fb} = U_H + U_{SC} \quad (4)$$

How the voltage is distributed across the semiconductor depletion region and the Helmholtz layer will depend on the capacitances associated with each (C_{SC}, C_H). Whenever U_H changes, the position of the valence band edge moves and changes the surface hole potential. Here, we find U_H for the

dx.doi.org/10.1021/ja503603k | J. Am. Chem. Soc. 2014, 136, 10632−10639

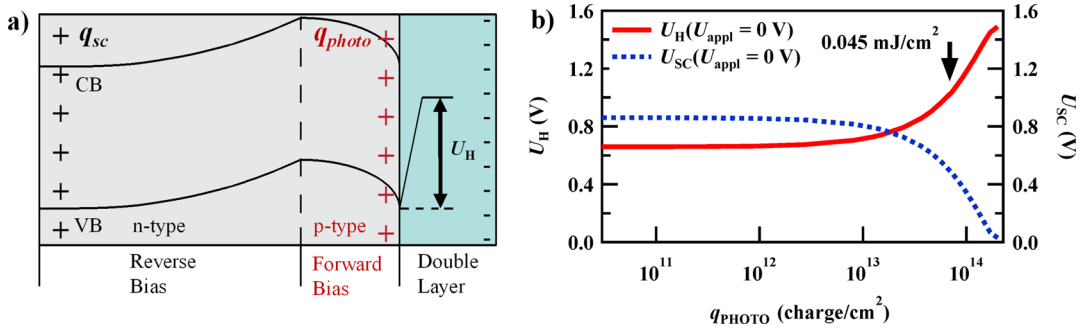

Figure 3. (a) Band diagram showing light-induced carrier inversion at the n-$SrTiO_3$ surface where photogenerated holes change n-$SrTiO_3$ to p-$SrTiO_3$. (b) Calculated Helmholtz voltage (U_H) and semiconductor (depletion layer) voltage (U_{SC}) as a function of photogenerated charges at the interface at U_{appl} = 0 V for n-$SrTiO_3$.

electrochemical conditions that apply to the in situ transient spectroscopy, namely a variable U_{appl} and high laser intensity.

At equilibrium, where U_{appl} = 0 V, and in the dark, U_H can be determined experimentally. As shown in Figure S4, Supporting Information, Mott−Schottky plots of the capacitance determine U_{fb} to be −1.52 V and photovoltage measurements determine U_{SC} to be 0.85 V. Together with eq 4, these measurements determine U_H to be 0.67 V. A detailed description of the methods used to determine these quantities are provided in the Supporting Information. Similar assessments have recently been made for another n-type semiconductor, Fe_2O_3.[33]

Intense light excitation alters the distribution of the voltage drop across C_{SC} and C_H. This is shown by the fact that the capacitance changes dramatically upon light excitation (Figure S5, Supporting Information). Rather than simply decreasing as the applied anodic voltage becomes less negative, as it does in the dark, the capacitance starts increasing beyond an anodic voltage intermediate between the flatband voltage (−1.52 V) and the photocurrent onset (−0.85 V, see Figure 1a). A detailed description of these measurements are provided in the Supporting Information. As depicted in Figure 3a, there are two types of surface charge densities (holes/cm^2) that contribute to the voltage-dependent capacitance in the semiconductor: q_{SC}, the hole density in the depletion layer dependent on U_{SC}, and q_{PHOTO}, induced by the laser pulse. Under laser excitation, the voltage drop that is present in the semiconductor under dark conditions is zeroed out by q_{PHOTO}, i.e., the semiconductor bands are flattened under illumination. As shown by the fast saturation of the photovoltage (Figure S4b, Supporting Information), very small laser fluences completely flatten the bands. This measurement indicates that only a small fraction of the photoinduced charge annihilates the voltage drop in the semiconductor, while most of the holes end up creating a thin, p-type layer at the interface that increases U_H. This carrier inversion process has been seen previously to move the valence band edge either as a result of a large number of surface defects[34] or under illumination,[28] as observed here.

Given the significant effect of these excess holes at the interface, U_H is a result of both q_{PHOTO} and q_{SC} screened by negatively charged ions in solution:

$$U_H = (q_{SC} + q_{PHOTO})/C_H \tag{5}$$

This construction has been applied successfully previously[23,35] for excess surface states and assumes a voltage-independent capacitance C_H. Here, q_{PHOTO} is obtained from the absorbed laser fluence and q_{SC} is given within the Schottky approximation by

$$q_{SC} = \sqrt{2\epsilon\epsilon_0|e_0|N_d\left(U_{SC} - \frac{k_BT}{|e_0|}\right)} \tag{6}$$

U_H can be self-consistently calculated from eqs 4, 5, and 6 for a variable U_{appl} and q_{PHOTO} to match the conditions of the in situ transient spectroscopy. C_H was determined from the equilibrium measurements in the dark, when U_{appl} and q_{PHOTO} are both zero. A U_{SC} = 0.85 V and U_H = 0.67 V give a C_H of 21 μF/cm^2. A detailed description of the methods used to determine these quantities is provided in the Supporting Information.

Figure 3b shows the results of the calculation for the 0.1% doped sample (2.66 × 10^{19} carriers/cm^3) at U_{appl} = 0 V and a variable q_{PHOTO}. At low q_{PHOTO}, the distribution across U_H and U_{SC} is essentially the same as in the dark at equilibrium. However, beyond a certain q_{PHOTO}, U_H increases substantially while U_{SC} concomitantly lowers. At the absorbed fluence used in the transient spectroscopy, 0.045 mJ/cm^2, ≈70% of the total U_{fb} drops across U_H.

Figure 4a shows how the magnitude of U_H changes as a function of U_{appl} for this laser fluence, at a somewhat higher laser fluence, and in the dark. While U_H increases roughly linearly with U_{appl} in the dark as well as under illumination, U_H is substantially higher and increases more strongly with U_{appl} under illumination. The two laser fluences show that variations in q_{PHOTO} in this fluence regime have only a moderate effect on how U_H depends on U_{appl}.

Figure 4b depicts the motion of the valence band edge with $U_H(U_{appl})$. $U_H(U_{appl})$ will be used to map how changes in the surface hole potential modulate the kinetics in the transient spectroscopy experiments. In addition to showing how the valence band edge moves with U_{appl}, $U_H(U_{appl})$ itself can be interpreted as the reaction free energy of reaction 2, as will be discussed further below. With the absolute potential of the valence band edge at equilibrium as a reference,[36] $U_H(U_{appl})$ determines the free energy difference between interfacial holes and O_2 evolution, or the overpotential η as described in the Supporting Information. As shown in Figure 4a, the overpotential ranges from ≈1.3 to 2.1 V for the laser fluences and applied potentials used in the in situ transient spectroscopy. This range is accessed by many n-type semiconductors used for photocatalytic water oxidation, characterized by low lying valence bands[36] with respect to the water oxidation potential, whether excited by UV or visible light.[33]

Open Circuit Kinetics of Interfacial Hole Transfer. The transient optical spectroscopy reported here was made sensitive to interfacial hole transfer by operating under conditions where

dx.doi.org/10.1021/ja503603k | J. Am. Chem. Soc. 2014, 136, 10632−10639

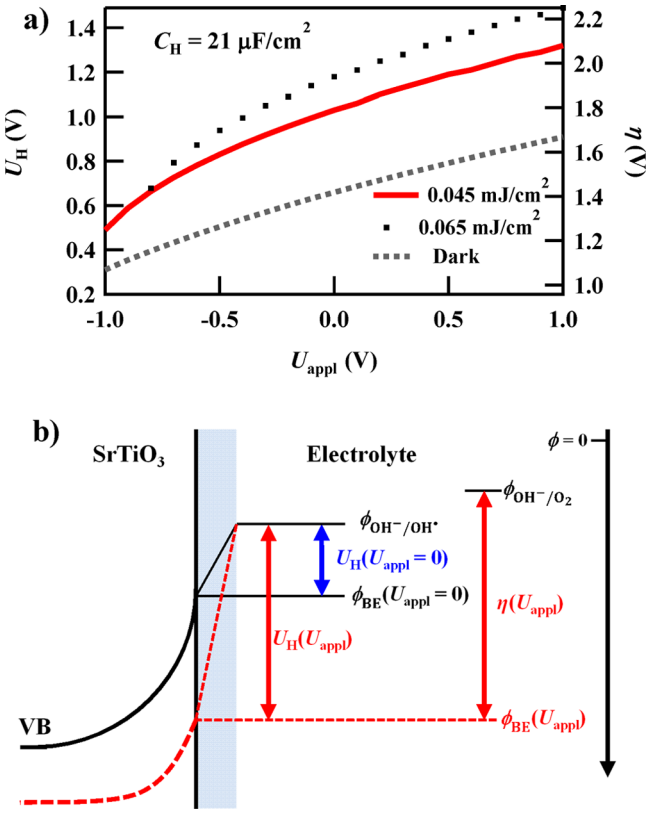

Figure 4. (a) Calculated Helmholtz voltage (U_H) as a function of applied potential with and without laser irradiation. The right-hand axis shows the corresponding overpotential (η) for water oxidation. (b) Graphical definition of interfacial potentials. ϕ's represent absolute potentials with respect to a reference electrode and U's represent potential differences, or voltage drops. The area shaded in blue indicates the Helmholtz layer.

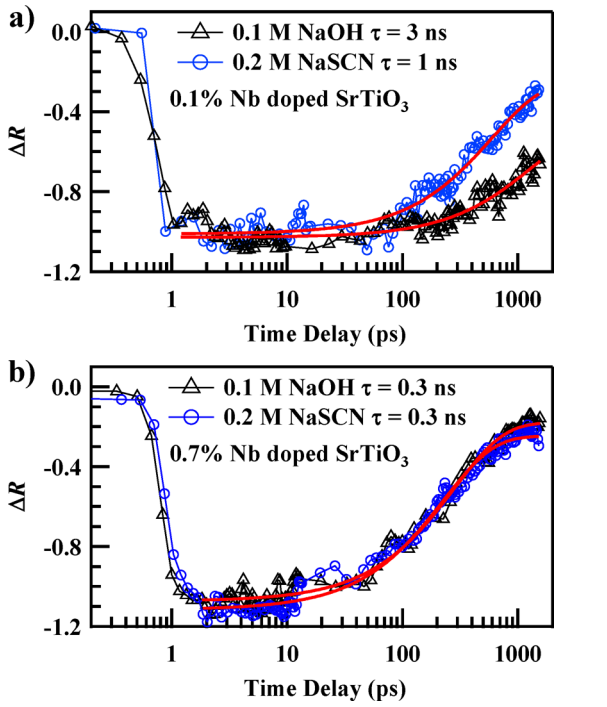

Figure 5. Normalized changes in reflectance, attributed to the decay of photogenerated holes, probed at 800 nm under open circuit conditions. The red lines represent single exponential fits to the data. Zero time delay between pump and probe was shifted to ≈1 ps for display of the data on a logarithmic time scale.

(1) essentially all excited electron–hole pairs are separated within the depletion layer and (2) the probe is only sensitive to carrier dynamics within the depletion layer width. The high quantum efficiency (>75%) for photocurrent for excitation wavelengths shorter than 300 nm is indicative of the first condition. To meet the latter condition, the experiments were performed in reflectance with a 45° incident angle. In such a reflectance geometry, the chosen near-infrared probe wavelength (800 nm), sensitive to free carrier excitation, only penetrates ≈25 nm from the surface according to[37] $d = \lambda/4\pi n$ and the measured index of refraction at 800 nm (Figure 1b). This penetration depth is equivalent to the depletion width for reverse bias conditions.

Figure 5a shows that the experimental conditions are in fact sensitive to interfacial charge transfer in 0.1% Nb-doped $SrTiO_3$ by comparing the transient response in aqueous electrolyte (NaOH) and in aqueous NaSCN electrolyte at open circuit. In both cases, we observe negative transient reflectance changes (ΔR) associated with an increase in the absorption of the material following photoexcitation of the semiconductor. Such an increase in absorption at optical frequencies corresponding to energies significantly lower than the band gap is typically assigned to the generation of free carriers, as has been done in $SrTiO_3$ previously.[38] Holes are the predominant free carrier generated within the depletion width by the excitation since the electrons are injected into the bulk of the semiconductor by the surface electric field faster than a few picoseconds (Supporting Information). The decrease in absorbance with time is then indicative of free holes leaving the semiconductor through the aqueous interface.

As shown by single exponential fits to the kinetics, the transient response in the aqueous NaSCN-electrolyte is three times faster than in the basic aqueous solution. The faster response in the NaSCN-electrolyte is attributed to the lower Nernstian potential for hole transfer to SCN^-,[39] a well-known hole scavenger. The significantly faster response in the NaSCN-electrolyte indicates that the interfacial charge transfer of free holes is preferentially being probed in our geometry where the depletion width, the excitation penetration depth, and the probe penetration depth are all matched to 25 nm. When the depletion width is smaller and not matched to the incoming light, as in the case for the 0.7% Nb-doped sample with a depletion width of 9 nm calculated by eq 3, the transient response (Figure 5b) does not change based on the solution potential.

The open circuit kinetics in Figure 5 are measured with no leads connecting the counter electrode to the anode. However, this does not imply that a voltage is not applied. From the photovoltage measurements, the pump excitation drops an equivalent of −0.85 V across the semiconductor, zeroing out the equilibrium U_{SC} in the dark and flattening the bands. This suggests another way to measure the open circuit kinetics, namely by applying −0.85 V when the circuit is closed. As long as this leads to U_{SC} = 0 V, the surface hole potential will be equivalent and guided by U_H. $U_H(U_{appl}$ = −0.85 V) is taken from the calculated U_H under illumination (Figure 4a) and consistently gives U_{SC} = 0 V according to eq 4. This shows that the true open circuit configuration and the circuit that applies −0.85 V between reference and working electrodes have equivalent surface hole potentials. These two circuit config-

dx.doi.org/10.1021/ja503603k | J. Am. Chem. Soc. 2014, 136, 10632–10639

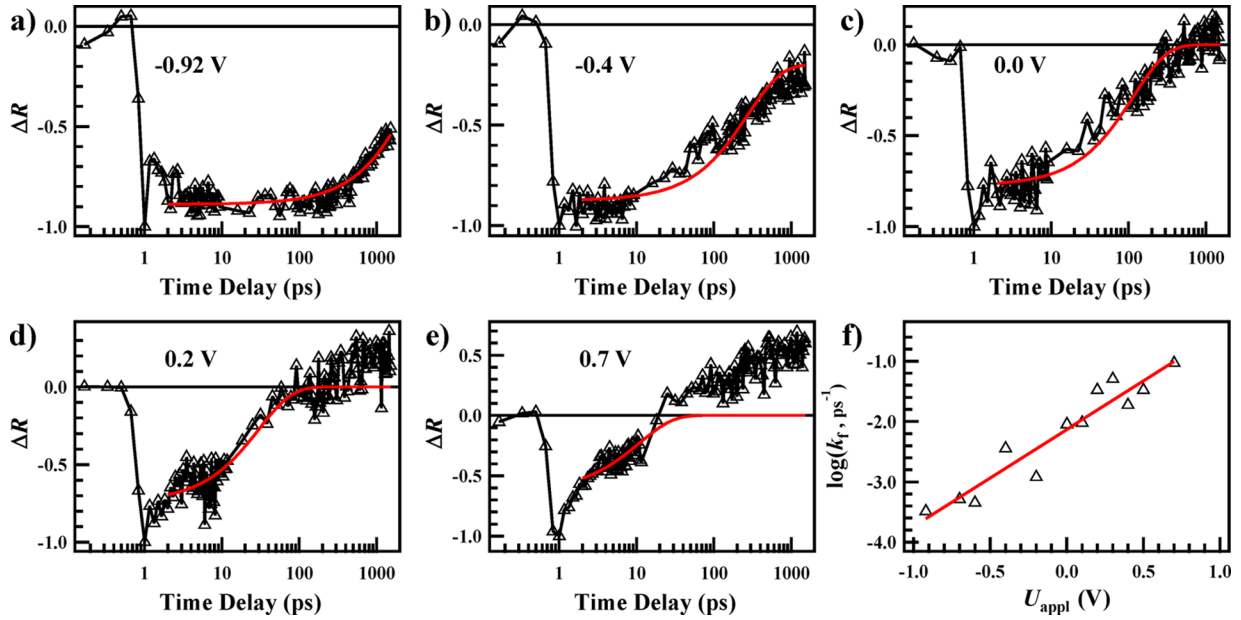

Figure 6. (a–e) Normalized transient reflectance changes, attributed to the decay of photogenerated holes, probed at 800 nm at the specified U_{appl}. The red lines are single exponential fits to the data. Zero time delay between pump and probe was shifted to ≈1 ps for display of the data on a logarithmic time scale. (f) Plot of $\log(k_f)$ vs U_{appl}. The red line is a linear fit to the data.

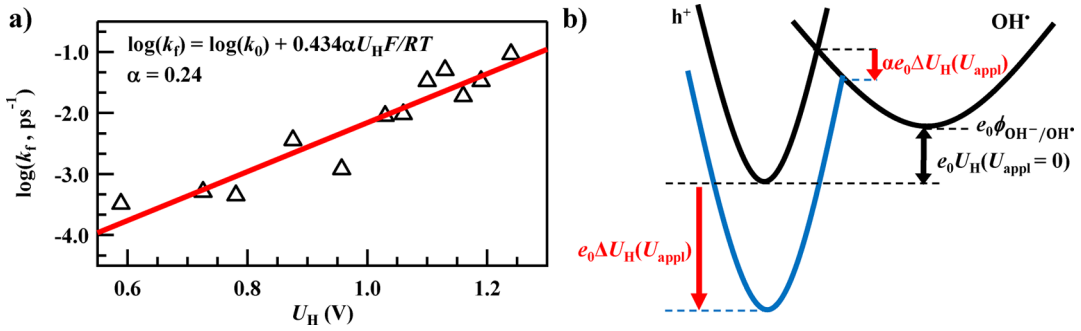

Figure 7. (a) Plot of $\log(k_f)$ vs Helmholtz voltage (U_H). U_H was calculated using an excitation fluence of 0.045 mJ cm^{-2} as described in the text. The red line is a linear fit to the data. The extracted transfer coefficient (α) is 0.24. (b) Diagram showing the free energy profile of the reaction.

urations yield the same transient response (Figure S6, Supporting Information), which means that the measured kinetics are truly dictated by the surface hole potential.

Kinetics of Interfacial Hole Transfer as a Function of Overpotential. We now turn to investigating these interfacial hole transfer kinetics as a function of changes in the surface hole potential due to valence band edge motion. As discussed in the Introduction, we consider the first hole transfer, namely the initial step in the cycle of water oxidation:

$$h^+ + OH^- \rightarrow OH^\bullet \quad (7)$$

Figure 6 shows the transient response (ΔR) for several representative applied potentials. Additional traces are provided in Figures S7 and S8, Supporting Information. The selected voltages are taken at points where the photocurrent onsets exponentially in the forward bias regime and where the photocurrent becomes potential-independent in the reverse bias regime (Figure 1a). For each voltage, the data could be nicely fit with a single exponential for negative ΔR, attributed to the decay of free holes. Such an exponential time dependence suggests a first order dependence of the above reaction on the concentration of holes. The time constant changes from 3 ns to 8 ps for applied voltages spanning −0.9 to 0.7 V.

Figure 6f displays how the logarithm of the rate constant depends on the applied voltage. As shown by the clear linear fit to $\log(k_f)$, the rate constant exponentially depends on the applied potential and demonstrates that we are measuring the rate of interfacial hole transfer as a function of surface hole potential, tuned by U_{appl}. The plot can be written in the form of an Arrhenius equation describing the activation barrier to this interfacial hole transfer:[19]

$$k_f = k_{OC}\exp(\alpha F(U_{appl} - U_{OC})/RT) \quad (8)$$

where R is the gas constant, F is the Faraday constant, and α is the phenomenological parameter that describes the shape of the activation barrier. k_{OC} is assigned to the kinetics at open circuit and U_{OC} is the equivalent applied voltage at open circuit conditions or −0.85 V as described in the previous section. As a check to analyzing the data in this way, we use the slope and the intercept of the plot (U_{appl} = 0 V) in Figure 6f, along with the kinetics measured at open circuit, to independently pull out U_{OC} using the transient kinetics alone. We find that the value agrees with U_{OC} = −0.85 V. This shows that the measured kinetics are truly tied to a potential tuned by the electrochemical cell in a manner that obeys the Arrhenius law.

dx.doi.org/10.1021/ja503603k | J. Am. Chem. Soc. 2014, 136, 10632−10639

While $\log(k_f)$ is linear with U_{appl}, the true potential at the surface changes with U_H. To obtain a physically meaningful measurement of α, we rescaled the voltage axis in Figure 6f with $U_H(U_{appl})$ in Figure 4a that determines the surface hole potential. The error in this rescaling of U_{appl} to $U_H(U_{appl})$ comes primarily from the error in the measurement of absorbed fluence. The rescaling is therefore done at two absorbed laser fluences, 0.045 mJ/cm^2 and 0.065 mJ/cm^2, where the actual absorbed laser fluence is estimated to fall between these two values. Here, the coefficient of the Arrhenius equation is set to be the equilibrium hole transfer rate at U_H = 0 V (k_0):

$$k_f = k_0 \exp(\alpha F U_H / RT) \quad (9)$$

While k_0 is not relevant to the determination of the slope and therefore α, it is an important parameter describing the activation barrier and will be discussed further below.

The results are shown in Figure 7a at a laser fluence of 0.045 mJ/cm^2 and give an α of 0.24. The results for the laser fluence of 0.065 mJ/cm^2 are shown in Figure S9, Supporting Information and give an α of 0.19. Given the uncertainty in the absorbed laser fluence, we report α = 0.20 ± 0.05. This means that only about 20% of the increase in surface hole potential is reflected in a decrease of the activation barrier for the reaction. Such an analysis leads to the asymmetric free energy diagram for interfacial charge transfer shown in Figure 7b. While α is commonly assumed to be 0.5, Marcus theory predicts a value different from 0.5, depending on the relative magnitude of overpotential and solvent reorganizational energy per molecule of reactant at the solid/electrolyte interface.[19] While a more detailed interpretation of α on a molecular level is left for future theoretical work, the value of α found here shows the strongly uphill free energy posed by transferring holes from a delocalized, O 2p valence band in the semiconductor to a localized OH^- ion at the aqueous interface. We note that the measured kinetics are obtained in a regime of high overpotential for the water oxidation reaction, covering ≈1.3 to 2.1 V (Figure 4a). In this regime, the initial hole transfer is not rate-limiting since changing the surface hole potential does not increase the photoinduced, steady-state current (Figure 1a).

In using the calculated U_H to determine α from the transient kinetics, only changes in U_H coming from the motion of the valence band edge are important. Therefore, α is independent of an assignment of the reaction taking place (reaction 7) and the magnitude of U_H. However, such a reaction is suggested by the fast picosecond time scales for hole transfer and the very basic conditions. Since the Helmholtz layer derives from OH^- screening the positive charge in the semiconductor, U_H is then interpreted as the free energy difference driving the $OH^-/OH^•$ reaction. Here, the OH^- ions are thought of as being located at the outer Helmholtz plane, rather than the inner plane describing directly absorbed species.[23] Using a reference for the valence band edge,[36] the data imply an absolute Nernstian potential for the $OH^-/OH^•$ reaction of +1.21 V vs normal hydrogen electrode (NHE) at pH = 13. This value can be compared with that obtained by gas-phase photoemission for the $OH^-/OH^•$ reaction 1.41 V vs NHE at pH = 13[40] as well as the range of values given by Hoare.[41] The similarity in these two values supports our assignment of reaction 7 to the measured kinetics. Further, the free energy difference driving the $OH^-/OH^•$ reaction at equilibrium conditions (U_{appl} = 0 V) in the dark was calculated for the TiO_2 (110) surface to be 0.57 V.[42] This can be compared with U_H = 0.67 V found experimentally here at equivalent conditions (Figure 4a). It is important to note, however, that the calculation assumes the OH species to be directly bound to the surface. Indeed, it is difficult to determine to what extent the inner Helmholtz rather than the outer Helmholtz layer is the potential difference responsible for the free energy difference, and we leave that as an open question.

In interpreting U_H as the free energy difference for the $OH^-/OH^•$ reaction, another parameter can be pulled out from the kinetic data, namely the kinetics of charge transfer at the Nernstian potential of the reaction or U_H = 0 V. This entails finding the x-intercept of Figure 7a and gives a value of $(6.76 \pm 1.50) \times 10^{-7}$ ps^{-1} for k_0. While α determines the shape of the activation barrier, k_0 relates to its magnitude. This value is critical to defining the current of a single step in the water oxidation reaction and would be essential to any model of the full O_2 evolving current. To our knowledge, there are no other direct measurements of this value in the literature, likely due to the fact that transient experiments on electrode reactions are scarce. Note, however, that extrapolating the intercept of the linear fit to our data assumes that eq 9 applies at low overpotentials for the water oxidation reaction, not directly accessible in these experiments.

The high overpotential range of water oxidation leading to fast, single exponential kinetics at early time scales has allowed for the observation of clear multicomponent kinetics within a short time window. The very fast component (below 2 ps) in the traces at applied potentials higher than 0.2 V (Figure 6) is tentatively attributed to hot hole transfer. At longer time scales, as shown in Figure 6 and in Figure S10, Supporting Information, ΔR changes sign indicating a new physical component to the kinetic response. This kinetic component is characterized by much longer time scales and does not show appreciable decay out to 1.5 ns. The results indicate that we are clearly resolving at least two kinetic components of the multifaceted water oxidation reaction. The observation of a single rate constant exponentially dependent on the surface hole potential that is followed by a second, much longer time scale suggests that a dominant new intermediate of the water oxidation reaction is formed upon picosecond hole transfer to OH^- within the Helmholtz layer. One possible intermediate is the surface oxo (=O) measured by steady-state infrared and Raman experiments previously.[9,16] Recently two types of oxo species, measured at millisecond time scales have been observed on cobalt oxide with transient FTIR spectroscopy.[16] Transient optical spectroscopy at ms time scales also indicates the formation of longer lived intermediates.[4,7] Future work will apply ultrafast infrared spectroscopy to this system to discover the appearance of the new intermediate that results from the disappearance of holes measured optically and at picosecond time scales here.

Here, we observed the kinetics of the first step of the water oxidation reaction in basic conditions, namely picosecond hole transfer to form a hydroxyl radical followed by the formation of a more stable intermediate. For the $OH^-/OH^•$ reaction, we have quantified for the first time the symmetry of the activation barrier through α and its magnitude through k_0 using an Arrhenius equation. We consistently derived a Nernstian potential for the reaction. Such a quantification informs electronic structure calculations that investigate the activation barriers and Nernstian potentials of each hole transfer of the water oxidation cycle.[11,13,14,43,44]

■ ASSOCIATED CONTENT

Supporting Information

SEM images showing laser-induced damage on 0.1% Nb doped $SrTiO_3$. Cyclic voltammograms of 0.1% Nb-doped $SrTiO_3$ in NaOH with and without irradiation by a xenon lamp. Steady-state photocurrent of 0.1% Nb-doped $SrTiO_3$ as a function of electrolyte pH. Mott−Schottky plots of 0.1% Nb-doped and 0.7% Nb-doped $SrTiO_3$ in the dark. Photovoltage measurements of 0.1% Nb-doped and 0.7% Nb-doped $SrTiO_3$ as a function of laser fluence. Differential capacitances measurements of 0.1% Nb-doped and 0.7% Nb-doped $SrTiO_3$ in 0.1 M Na_2SO_4 with and without laser irradiation. Kinetics traces for 0.1% Nb-doped $SrTiO_3$ under open circuit condition and with an applied bias of −0.85 V. Additional kinetics traces at various applied potentials. Plot of $\log(k_f)$ vs Helmholtz potential drop (U_H) for a higher fluence. Kinetic traces plotted on a linear time scale. Descriptions of methods used to determine the potential distribution at the semiconductor/liquid interface, the differential capacitance measurements under light excitation, and the determination of overpotentials. Estimation of the drift velocity of holes in the depletion layer. This material is available free of charge via the Internet at http://pubs.acs.org.

■ AUTHOR INFORMATION

Corresponding Author

tanjacuk@berkeley.edu

Notes

The authors declare no competing financial interest.

■ ACKNOWLEDGMENTS

This material is based upon work supported by the Air Force Office of Scientific Research under AFOSR award no. FA9550-12-1-0337 and by the Department of Energy Office of Basic Energy Sciences, under the CPIMS program KC030102 (FWP no. CH12CUK1). Work (ellipsometry measurement) at the Molecular Foundry was supported by the Office of Science, Office of Basic Energy Sciences, of the U.S. Department of Energy under contract no. DE-AC02-05CH11231. We thank Adam Schwartzberg for helping us with the ellipsometry measurements. We thank Heinz Frei, Steven Leone, and Gabor Somorjai for critically reading the manuscript and Dunwei Wang for helpful comments on our steady-state measurements.

■ REFERENCES

(1) Kasinski, J. J.; Gomez-Jahn, L. A.; Faran, K. J.; Gracewski, S. M.; Miller, R. J. D. *J. Chem. Phys.* **1989**, *90*, 1253−1269.

(2) Lantz, J. M.; Corn, R. M. *J. Phys. Chem.* **1994**, *98*, 9387−9390.

(3) Nakamura, R.; Nakato, Y. *J. Am. Chem. Soc.* **2004**, *126*, 1290−1298.

(4) Tang, J.; Durrant, J. R.; Klug, D. R. *J. Am. Chem. Soc.* **2008**, *130*, 13885−13891.

(5) McAlpin, J. G.; Surendranath, Y.; Dincă, M.; Stich, T. A.; Stoian, S. A.; Casey, W. H.; Nocera, D. G.; Britt, R. D. *J. Am. Chem. Soc.* **2010**, *132*, 6882−6883.

(6) Surendranath, Y.; Kanan, M. W.; Nocera, D. G. *J. Am. Chem. Soc.* **2010**, *132*, 16501−16509.

(7) Cowan, A. J.; Barnett, C. J.; Pendlebury, S. R.; Barroso, M.; Sivula, K.; Grätzel, M.; Durrant, J. R.; Klug, D. R. *J. Am. Chem. Soc.* **2011**, *133*, 10134−10140.

(8) Sivasankar, N.; Weare, W. W.; Frei, H. *J. Am. Chem. Soc.* **2011**, *133*, 12976−12979.

(9) Yeo, B. S.; Bell, A. T. *J. Am. Chem. Soc.* **2011**, *133*, 5587−5593.

(10) Huang, Z.; Lin, Y.; Xiang, X.; Rodrguez-Córdoba, W.; McDonald, K. J.; Hagen, K. S.; Choi, K.-S.; Brunschwig, B. S.; Musaev, D. G.; Hill, C. L.; Wang, D.; Lian, T. *Energy Environ. Sci.* **2012**, *5*, 8923−8926.

(11) Su, H.-Y.; Gorlin, Y.; Man, I. C.; Calle-Vallejo, F.; Nørskov, J. K.; Jaramillo, T. F.; Rossmeisl, J. *Phys. Chem. Chem. Phys.* **2012**, *14*, 14010−14022.

(12) Cooper, J. K.; Ling, Y.; Longo, C.; Li, Y.; Zhang, J. Z. *J. Phys. Chem. C* **2012**, *116*, 17360−17368.

(13) Liao, P.; Keith, J. A.; Carter, E. A. *J. Am. Chem. Soc.* **2012**, *134*, 13296−13309.

(14) Bajdich, M.; García-Mota, M.; Vojvodic, A.; Nørskov, J. K.; Bell, A. T. *J. Am. Chem. Soc.* **2013**, *135*, 13521−13530.

(15) Bediako, D. K.; Surendranath, Y.; Nocera, D. G. *J. Am. Chem. Soc.* **2013**, *135*, 3662−3674.

(16) Zhang, M.; de Respinis, M.; Frei, H. *Nat. Chem.* **2014**, *6*, 362−367.

(17) Harriman, A.; Pickering, I. J.; Thomas, J. M.; Christensen, P. A. *J. Chem. Soc., Faraday Trans. 1* **1988**, *84*, 2795−2806.

(18) Lin, X.; Hu, X.; Concepcion, J. J.; Chen, Z.; Liu, S.; Meyer, T. J.; Yang, W. *Proc. Natl. Acad. Sci. U.S.A.* **2012**, *109*, 15669−15672.

(19) Bard, A. J.; Faulkner, L. R. *Electrochemical Methods: Fundamentals and Applications*, 2nd ed.; Wiley: Hoboken, NJ, 2000.

(20) Newman, J.; Thomas-Alyea, K. E. *Electrochemical Systems*, 3rd ed.; Wiley: Hoboken, NJ, 2004.

(21) Jaeger, C. D.; Bard, A. J. *J. Phys. Chem.* **1979**, *83*, 3146−3152.

(22) Norton, A. P.; Bernasek, S. L.; Bocarsly, A. B. *J. Phys. Chem.* **1988**, *92*, 6009−6016.

(23) Green, M. *J. Chem. Phys.* **1959**, *31*, 200−203.

(24) De Gryse, R.; Gomes, W. P.; Cardon, F.; Vennik, J. *J. Electrochem. Soc.* **1975**, *122*, 711−712.

(25) Uosaki, K.; Kita, H. *J. Electrochem. Soc.* **1983**, *130*, 895−897.

(26) Cooper, G.; Turner, J. A.; Parkinson, B. A.; Nozik, A. J. *J. Appl. Phys.* **1983**, *54*, 6463−6473.

(27) van de Krol, R.; Grätzel, M. *Photoelectrochemical Hydrogen Production*; Springer: New York, NY, 2012; Vol. *102*, pp 13−67.

(28) Turner, J. A.; Manassen, J.; Nozik, A. J. *Appl. Phys. Lett.* **1980**, *37*, 488−491.

(29) Stoian, R.; Rosenfeld, A.; Ashkenasi, D.; Hertel, I. V.; Bulgakova, N. M.; Campbell, E. E. B. *Phys. Rev. Lett.* **2002**, *88*, 097603.

(30) Roeterdink, W. G.; Juurlink, L. B. F.; Vaughan, O. P. H.; Diez, J. D.; Bonn, M.; Kleyn, A. W. *Appl. Phys. Lett.* **2003**, *82*, 4190.

(31) de Kreuk, C.; de Groot, J.; Mackor, A. *Sol. Energy Mater.* **1981**, *5*, 437−444.

(32) Bocarsly, A. B.; Bolts, J. M.; Cummins, P. G.; Wrighton, M. S. *Appl. Phys. Lett.* **1977**, *31*, 568.

(33) Du, C.; Yang, X.; Mayer, M. T.; Hoyt, H.; Xie, J.; McMahon, G.; Bischoping, G.; Wang, D. *Angew. Chem., Int. Ed.* **2013**, *52*, 12692−12695.

(34) Bard, A. J.; Bocarsly, A. B.; Fan, F. R. F.; Walton, E. G.; Wrighton, M. S. *J. Am. Chem. Soc.* **1980**, *102*, 3671−3677.

(35) Bockris, J. O. M.; Khan, S. U. M. *Surface Electrochemistry,*; Springer: New York, NY, 1993; Chpt. 2, pp 59−202.

(36) Xu, Y.; Schoonen, M. A. A. *Am. Mineral.* **2000**, *85*, 543−556.

(37) Fishman, I. M.; Marshall, C. D.; Meth, J. S.; Fayer, M. D. *J. Opt. Soc. Am. B* **1991**, *8*, 1880−1888.

(38) Yamada, Y.; Yasuda, H.; Tayagaki, T.; Kanemitsu, Y. *Appl. Phys. Lett.* **2009**, *95*, 121112.

(39) Wardman, P. *J. Phys. Chem. Ref. Data* **1989**, *18*, 1637−1755.

(40) Koppenol, W. H.; Liebman, J. F. *J. Phys. Chem.* **1984**, *88*, 99−101.

(41) Hoare, J. P. *Standard Potentials in Acqueous Solution*; Bard, A. J., Parsons, R., Eds.; IUPAC: New York, NY, 1985; pp 49−63.

(42) Cheng, J.; Sulpizi, M.; VandeVondele, J.; Sprik, M. *ChemCatChem* **2012**, *4*, 636−640.

(43) Liu, F.; Concepcion, J. J.; Jurss, J. W.; Cardolaccia, T.; Templeton, J. L.; Meyer, T. J. *Inorg. Chem.* **2008**, *47*, 1727−1752.

(44) Alibabaei, L.; Brennaman, M. K.; Norris, M. R.; Kalanyan, B.; Song, W.; Losego, M. D.; Concepcion, J. J.; Binstead, R. A.; Parsons, G. N.; Meyer, T. J. *Proc. Natl. Acad. Sci. U.S.A.* **2013**, *110*, 20008−20013.